DEU FMD 26(77) 2024, 218-230

Dokuz Eylül Üniversitesi Mühendislik Fakültesi Fen ve Mühendislik Dergisi
Dokuz Eylul University Faculty of Engineering Journal of Science and Engineering
Elektronik/Online ISSN: 2547-958X

RESEARCH ARTICLE / ARAŞTIRMA MAKALESI

Gravity Tensors and Moho Depth Variations of the Region between West Italy and Eastern of Caspian Sea

Batı İtalya ile Hazar Denizi Doğusu Arasındaki Bölgenin Gravite Tensörleri ve Moho Derinlik Değişimleri

Fikret Doğru [1*], Oya Pamukçu [2]

[1] Atatürk Üniversitesi Oltu Meslek Yüksekokulu İnşaat Bölümü, Erzurum, TÜRKİYE
[2] Dokuz Eylül Üniversitesi Mühendislik Fakültesi Jeofizik Mühendisliği Bölümü, İzmir, TÜRKİYE

Corresponding Author / Sorumlu Yazar *: fikretdogru@atauni.edu.tr

Abstract

The crust structure of the region from the west of Italy to the east of the Caspian Sea was examined within the scope of this study. In addition, the effect of both the shallow and deep structure were revealed by calculating the gravity tensors of the region in different degrees. For this purpose, the spherical free air gravity anomaly of the region was first calculated. The combination of EGM2008 and GOCE DIR R4 models were used for this calculation. Then the gravity tensors of the region were calculated separately using only EGM2008 model and only GOCE DIR R4. The spherical free air anomaly of the region was calculated using the topographic model. The spherical Bouguer anomaly of the region was obtained by subtracting the anomaly obtained from this topographic model from the spherical free air anomaly obtained from GOCE DIR R4 + EGM2008 combined model. The radial averaged power spectrum of the spherical Bouguer anomaly was taken and the anomaly thought to be caused by Moho was filtered out. Moho depth map of the whole region was obtained by applying the Parker-Oldenburg inversion to the filtered anomaly. The obtained values were compared with previous studies and found to be compatible.

Keywords: *Tensor, GOCE, EGM2008, Bouguer, Moho.*

Öz

İtalya'nın batısından Hazar Denizi'nin doğusuna kadar olan bölgenin kabuk yapısı bu çalışma kapsamında incelenmiştir. Ayrıca bölgenin farklı derecelerdeki gravite tensörleri hesaplanarak hem sığ hem de derin yapının etkisi ortaya konulmuştur. Bu amaçla öncelikle bölgenin küresel serbest hava gravite anomalisi hesaplanmıştır. Bu hesaplama için EGM2008 ve GOCE DIR R4 modellerinin kombinasyonu kullanılmıştır. Daha sonra sadece EGM2008 modeli ve sadece GOCE DIR R4 modeli kullanılarak bölgenin gravite tensörleri ayrı ayrı hesaplanmıştır. Topografik model kullanılarak bölgenin küresel serbest hava anomalisi hesaplanmıştır. Bu topografik modelden elde edilen anomalinin GOCE DIR R4 + EGM2008 birleşik modelinden elde edilen küresel serbest hava anomalisinden çıkarılmasıyla bölgenin küresel Bouguer anomalisi elde edilmiştir. Küresel Bouguer anomalisinin radyal ortalamalı güç spektrumu alınmış ve Moho'nun neden olduğu düşünülen anomali filtrelenmiştir. Bu Moho'nun neden olduğu düşünülen anomaliye ters çözüm uygulanarak tüm bölgeye ait Moho derinlik haritası elde edilmiştir. Elde edilen değerler önceki çalışmalarla karşılaştırılmış ve uyumlu olduğu görülmüştür.

Anahtar Kelimeler: *Tensör, GOCE, EGM2008, Bouguer, Moho.*

1. Introduction

In the study area as shown in Figure 1, there are large tectonic lines and local kinematic structures created by these tectonic lines. The region under the influence of the Alpine Himalayan belt from west to east consists of terrestrial and marine parts [1-3]. The Hellenic arc is in a very active region especially in the marine part [4-6]. The western extension tectonics throughout Anatolia, the North Anatolian Fault Zone in the north, the East Anatolian Fault Zone in the southerneast, the Bitlis Zagros suture zone extending to Iran and the Dead Sea fault in the south are the characteristic tectonic elements of the region. Within the scope of this study, the aim is to examine the continuity of the structures by looking at the area in Figure 1 from a wider perspective. To this end, data gathered from satellite-based gravity models were used.

DOI:10.21205/deufmd.2024267704

Atıf şekli / How to cite:

Dogru, F., Pamukcu, O. (2024). G ravity Tensors and Moho Depth Variations of the Region between West Italy and Eastern of Caspian Sea. 26(76), 218-230.

Geliş Tarihi / Received: 22.03.2023
Kabul Tarihi / Accepted: 02.08.2023

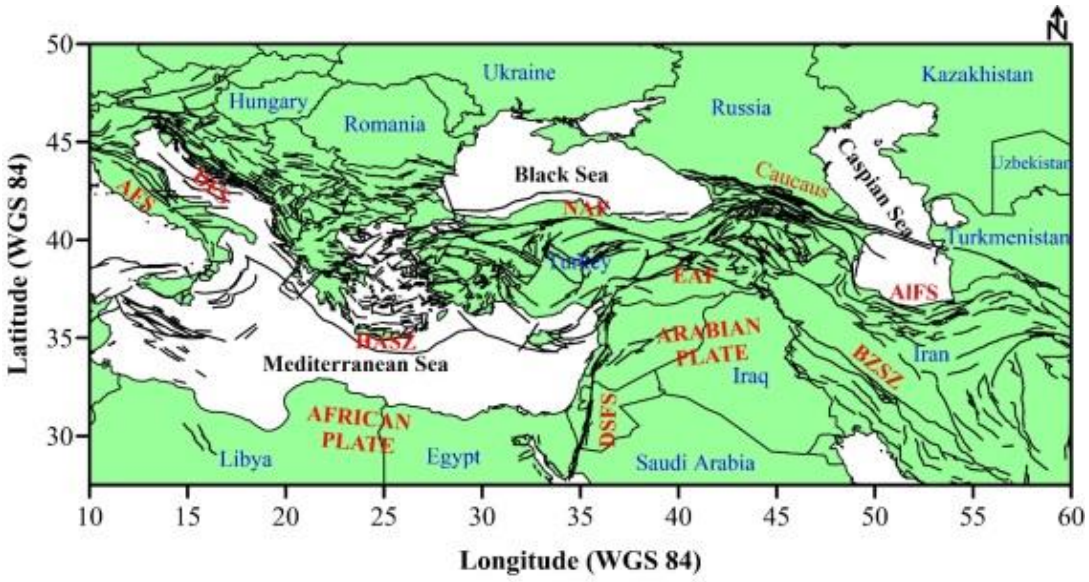

Figure 1. Tectonic framework of the study area (AFS:Apennines Fault System; AlFS: Alborz Fault System; BZSZ: Bitlis Zagros Suture Zone; DFZ: Dinarides Fault System; DSFS: Dead Sea Fault System; EAF: Eastern Anatolia Fault; HASZ: Hellenic Arc Subduction Zone; NAF: North Anatolian Fault) (Global active faults are taken from [7]).

The comparison of satellite based gravity anomaly and terrestrial gravity anomaly at the same elevation was made for the Aegean Sea and western Anatolia by the study of Dogru et al., [8]. In this study, the results show that the lowest root mean square error between satellite based gravity anomaly and terrestrial data was obtained from the combination of GOCE Direct Release 4 [9] and Earth Gravitational Model 2008 (EGM2008) [10]. Therefore, a combination of GOCE Direct Release 4 [9] and Earth Gravitational Model 2008 (EGM2008) [10] models were selected and used to calculate the free air gravity data of the region. Anomaly between the degree of 2-2190 was obtained by calculating the GOCE model up to degree of 240 and using EGM2008 up to the degree of 241-2190. Afterwards, the free air gravity anomaly of the region was calculated from the dV_ELL_Earth2014_plusGRS80 [11] topographic model. Then, topographic free air gravity anomaly was extracted from the spherical free gravity anomaly calculated from GOCE DIR R4 + EGM2008 model. Thus, the spherical Bouguer gravity anomaly of the region was obtained. Finally, the gravity tensors and Moho depth values of the region were obtained. In addition, tensor analysis of EGM2008 and GOCE DIR R4 data was performed and the results were examined among themselves. As a result, the variations in Moho depths and tensor values determined in this study were evaluated together with regional tectonic elements.

2. Materials and Method

2.1. Spherical gravity anomaly calculation

In this study, free air gravity anomalies are calculated using the following equations [12]:

$$\Delta g_{sa}(r,\varphi,\lambda) = -\frac{\partial T(r,\varphi,\lambda)}{\partial r} - \frac{2}{r}T(r,\varphi,\lambda) = \frac{GM}{r^2}\sum_{n=n_{min}}^{n_{max}}\left(\frac{R}{r}\right)^n (n-1)\sum_{m=0}^{n}\left(\Delta\bar{C}_{n,m}cosm\lambda + \Delta\bar{S}_{n,m}sinm\lambda\right)\bar{P}_{n,m}(sin\varphi) \quad (1)$$

In this formula, r, φ and λ are spherical radius, latitude and longitude; n, m are spherical harmonic degrees and order; n_{min} and n_{max} are the degree of minimum and maximum spherical harmonic expansion; $\bar{P}_{n,m}(sin\varphi)$ is the 4π complete normalization associated with the Legendre function; GM and r represent the gravity constant of the geocentric and the radius of the reference sphere. $\bar{C}_{n,m}$ and $\bar{S}_{n,m}$ are the 4π fully normalized spherical harmonic coefficients, $\Delta\bar{C}_{n,m}$ and $\Delta\bar{S}_{n,m}$ represent the difference between the harmonic coefficients in the gravity model and the harmonic coefficients of the normal gravity field. GrafLab (Gravity field laboratory), which is a MATLAB-based program, was used in the calculation of anomalies [12].

2.2. Tensors of spherical gravity anomalies

Gravity tensors are calculated as shown below [12]:

$$T(r,\varphi,\lambda) = \begin{pmatrix} T_{xx} & T_{xy} & T_{xz} \\ T_{yx} & T_{yy} & T_{yz} \\ T_{zx} & T_{zy} & T_{zz} \end{pmatrix} \quad (2)$$

Calculation formulas of gravity tensors are given in the supplementary file.

2.3. Radial Averaged Power Spectrum

The most important feature of the radial averaged power spectrum is that it shows the correct changes at different slopes in different radial wave number patterns. Generally, small radial wave numbers are represented by deeper, medium wave numbers by shallow sources and high wave numbers by noise in the data [13-15]. The depth of each equivalent layer is calculated as follows:

$$h = \frac{B(kr_1) - B(kr_2)}{4\pi(kr_2 - kr_1)} \quad (3)$$

Here; kr_1 and kr_2 are the starting and ending radial wave numbers of the overlapping line, $B(kr_1)$ and $B(kr_2)$ are the radial averaged natural logarithmic power spectrum values corresponding to these wave numbers [16]. The radial amplitude (A) is calculated as the averaged of the 2D Fourier amplitude spectrum (F) with radius $kr = \left[k_x^2 + k_y^2\right]^{1/2}$ centered at the starting point and expressed as $A = |F| = [Re(F)^2 + Im(F)^2]^{1/2}$ [17-18].

2.4. Parker-Oldenburg inversion

Parker-Oldenburg algorithm was applied to the spherical Bouguer anomaly obtained as a result of bandpass filter by using kr values in the previous application [19-20]. The Fourier transform of spherical Bouguer gravity anomalies (Δg_{BA}) is obtained using the equation proposed by Parker [19]:

$$\mathfrak{F}(\Delta g_{BA}) = -2\pi G\rho e^{(-kz_0)} \sum_{n=1}^{\infty} \frac{k^{n-1}}{n!} \; f[h^n(x)] \tag{4}$$

Here, $\mathfrak{F}(\Delta g_{BA})$ represents the Fourier transform of the gravity anomaly, G universal gravitational constant, ρ density contrast, k wave number, $h^n(x)$ downward continuation depth and z_0 mean depth. Oldenburg [20] rearranged equation (4) to determine the depth of the structure from the gravity anomaly iteratively:

$$\mathfrak{F}[h(x)] = -\frac{\mathfrak{F}[\Delta g(x)]e^{(-kz_0)}}{2\pi G\rho} - \sum_{n=2}^{\infty} \frac{k^{n-1}}{n!} f[h^n(x)] \tag{5}$$

2.5. Upward continuation

Upward continuation is a method that transforms anomalies measured on one surface into those that would have been measured on some higher surface. The upward-continued anomalies do not provide direct information about the source, but they can be instructive nonetheless. In particular, the process of upward continuation tends to attenuate anomalies caused by local, near-surface sources relative to anomalies caused by deeper, more profound sources. The potential data at two observation heights are related by the upward continuation operation [21],

$$T_h(x, y, \Delta h) = \frac{1}{2\pi} \int_{-\infty}^{\infty} \int_{-\infty}^{\infty} \frac{T_o(x', y', \Delta h)}{[(x' - x)^2 + (y' - y)^2 + \Delta h^2]^{3/2}} dx' dy' \tag{6}$$

where $T_o(x, y)$ and $T_h(x, y, h)$) are respectively the potential data at two observation heights separated by a vertical distance Δh. Applying a two-dimensional Fourier transform to equation (6) yields a simpler form in which the Fourier transforms of the two quantities are related to each other by a simple upward continuation operator,

$$\tilde{T}_h(\omega_x, \omega_y, \Delta h) = e^{-\Delta h \omega_r} \tilde{T}_o(\omega_x, \omega_y) \tag{7}$$

Where $\tilde{T}_o(\omega_x, \omega_y)$ denotes the Fourier transform of $T_o(x, y)$, (ω_x, ω_y) are wavenumbers in x and y direction and $\omega_r = \sqrt{\omega_x^2 + \omega_y^2}$ is the radial wavenumber. The upward continuation operator attenuates with height the high frequency content of a potential anomaly.

3. Results

First of all, the spherical free air anomaly of the area in Figure 1 was calculated (Figure 2) and then the Bouguer anomaly was calculated using the topography model (Figure 3). The topographic elevation values of the region reach up to 5000 meters. Spherical free air anomaly values vary between 250 mGal and -200 mGal. It is seen that spherical free air anomalies were obtained positive high values especially in the Caucasus where the topographic height is high, along the Iran-Caspian Sea coast and in the vicinity of Cyprus. Spherical free air anomalies were observed negatively in the sea areas as expected. Spherical Bouguer gravity anomaly values vary between 280 mGal and -200 mGal. Contrary to spherical free air anomalies, positive high values were observed in seas and negative anomalies were observed in lands.

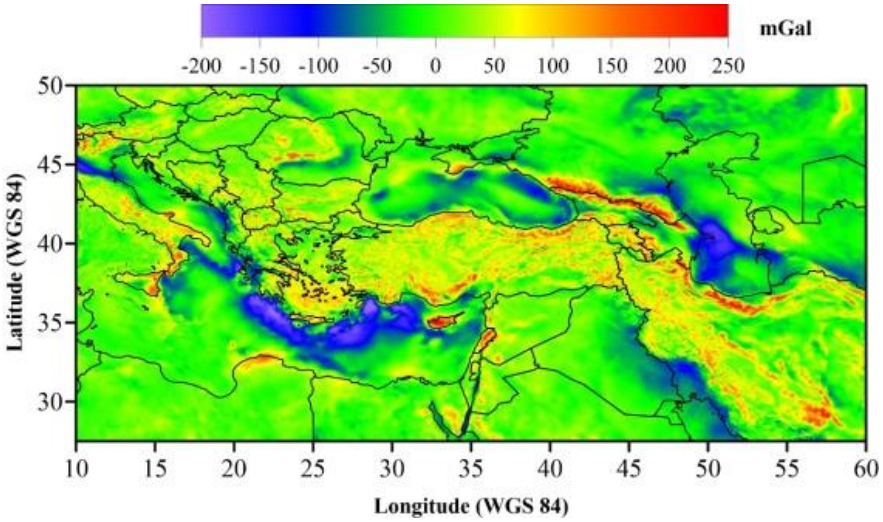

Figure 2. Spherical free air gravity anomaly with the combination of EGM2008 and GOCE DIR R4 model.

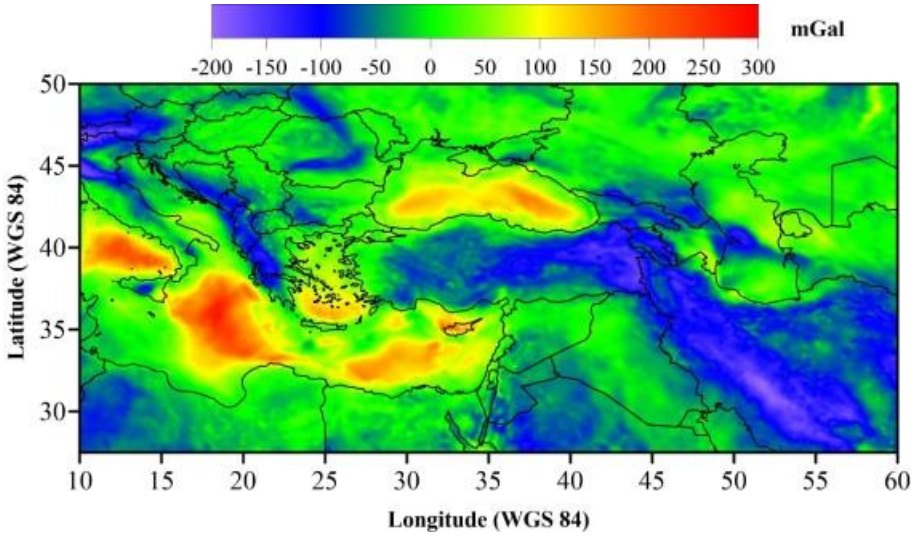

Figure 3. Spherical Bouguer gravity anomaly of the study area.

Afterwards, the difference between EGM2008 and GOCE DIR R4 models up to 240 degrees/order (2 to 240) was calculated for the whole region (Figure 4). It is seen that values are between -40 and +30 in eastern Egypt and in southwest Israel but when this anomaly was eliminated values are between approximately -18 and +18 in the rest of the region.

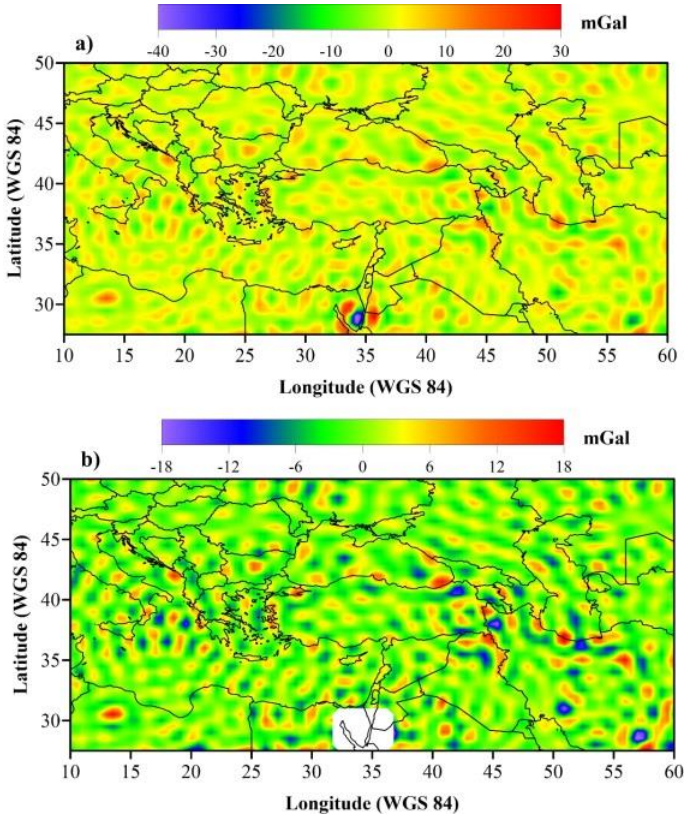

Figure 4. a) The difference between EGM2008 and GOCE DIR R4 (up to degree/order 2 to 240) and b) maximum value area middle in the South is blanked to show maximum and minimum difference of the whole area.

Gravity tensors were first calculated from the satellite model of EGM2008 (Figures 5a, 6a, 7a, 8a, 9a and 10a). In addition, upward extension was applied to the EGM2008 tensor data (Figures 5b, 6b, 7b, 8b, 9b and 10b). In addition, tensors have been calculated from GOCE Direct model (Release 4) up to degree/order 2 to 240 (Figures 5c, 6c, 7c, 8c, 9c and 10c). In this way, both tensors of deep structure effects originating from low frequency and wide wavelength and tensors of shallow structure effects originating from high frequencies and short wavelengths were obtained.

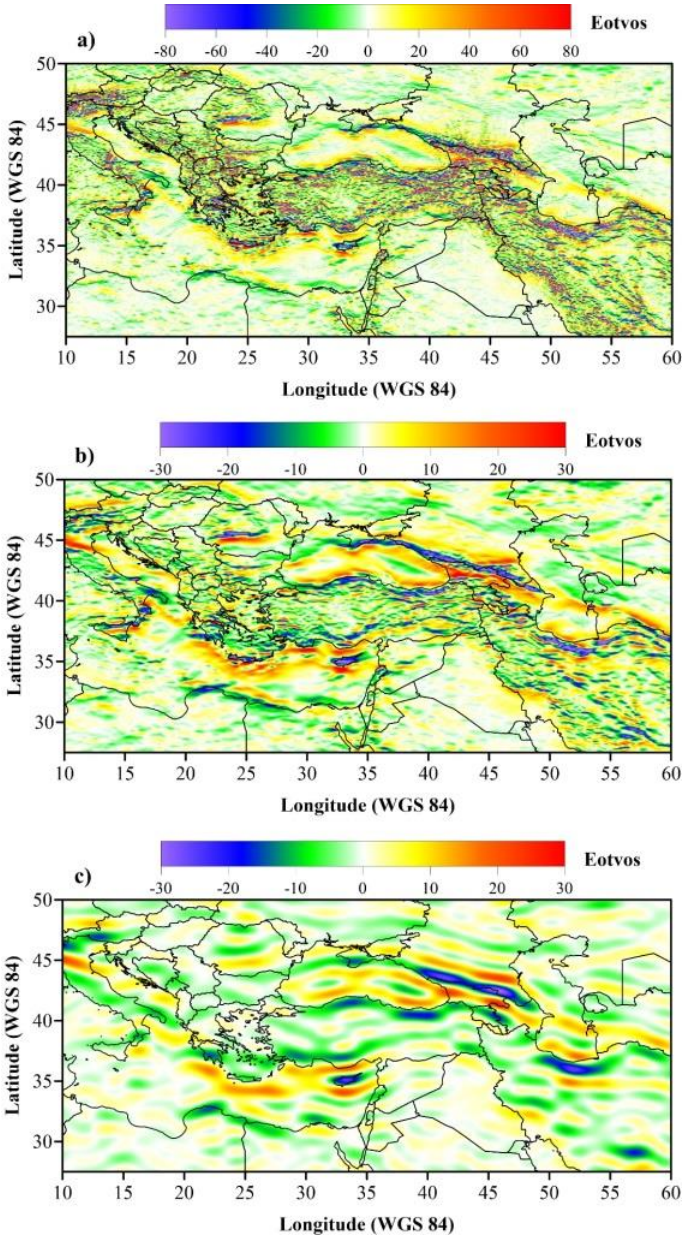

Figure 5. a) Txx tensor of EGM2008 up to degree 2190, b) Upward continuation of Txx tensor of EGM2008 and c) Txx tensor of GOCE DIR R4 up to degree 240.

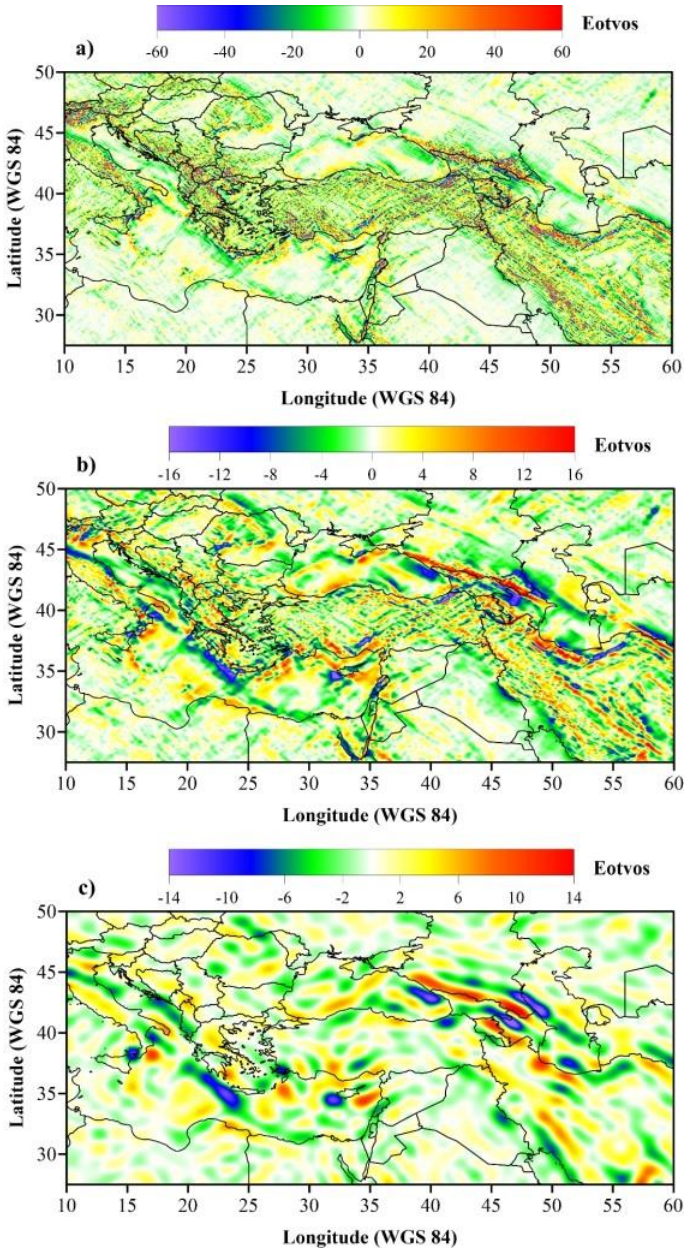

Figure 6. a) Txy tensor of EGM2008 up to degree 2190, b) Upward continuation of Txy tensor of EGM2008 and c) Txy tensor of GOCE DIR R4 up to degree 240.

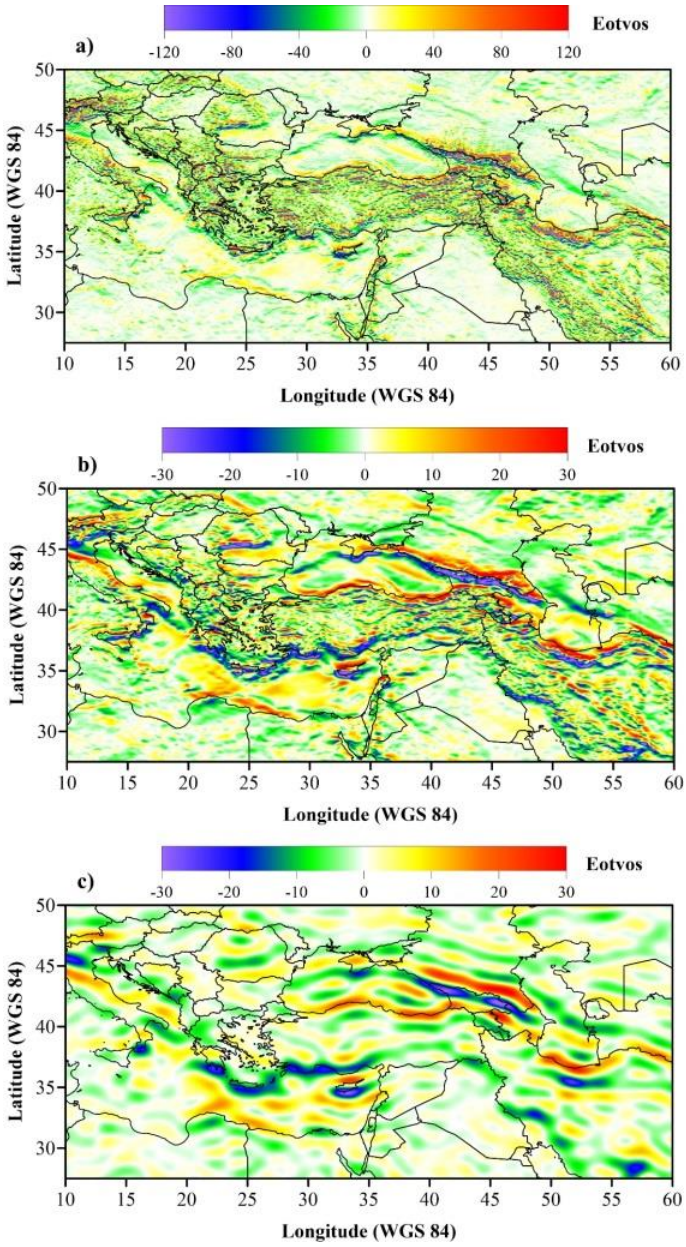

Figure 7. a) Txz tensor of EGM2008 up to degree 2190, b) Upward continuation of Txz tensor of EGM2008 and c) Txz tensor of GOCE DIR R4 up to degree 240.

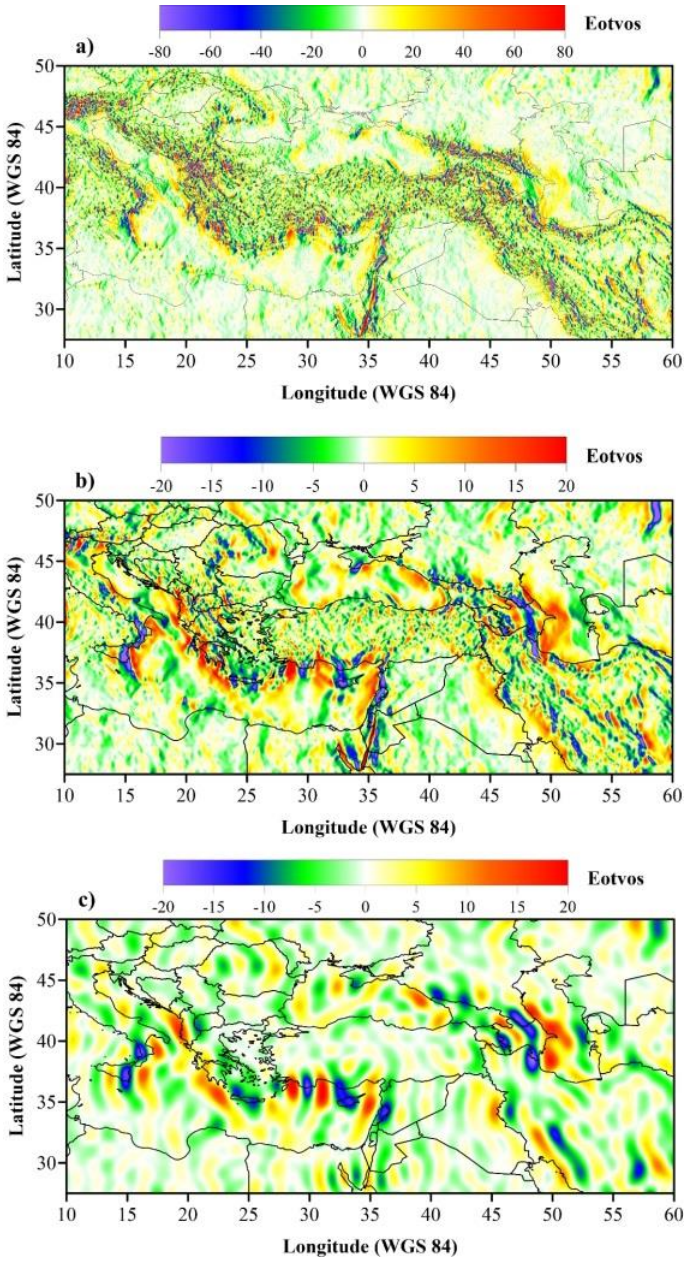

Figure 8. a) Tyy tensor of EGM2008 up to degree 2190, b) Upward continuation of Tyy tensor of EGM2008 and c) Tyy tensor of GOCE DIR R4 up to degree 240.

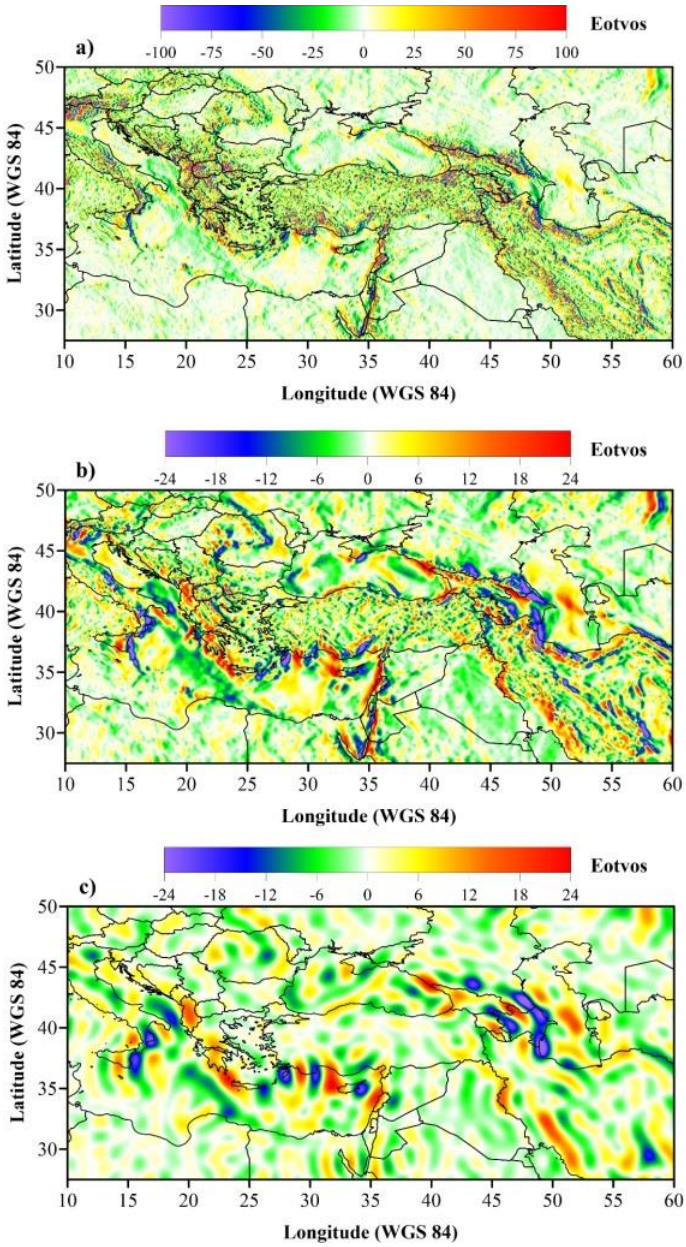

Figure 9. a) Tyz tensor of EGM2008 up to degree 2190, b) Upward continuation of Tyz tensor of EGM2008 and c) Tyz tensor of GOCE DIR R4 up to degree 240.

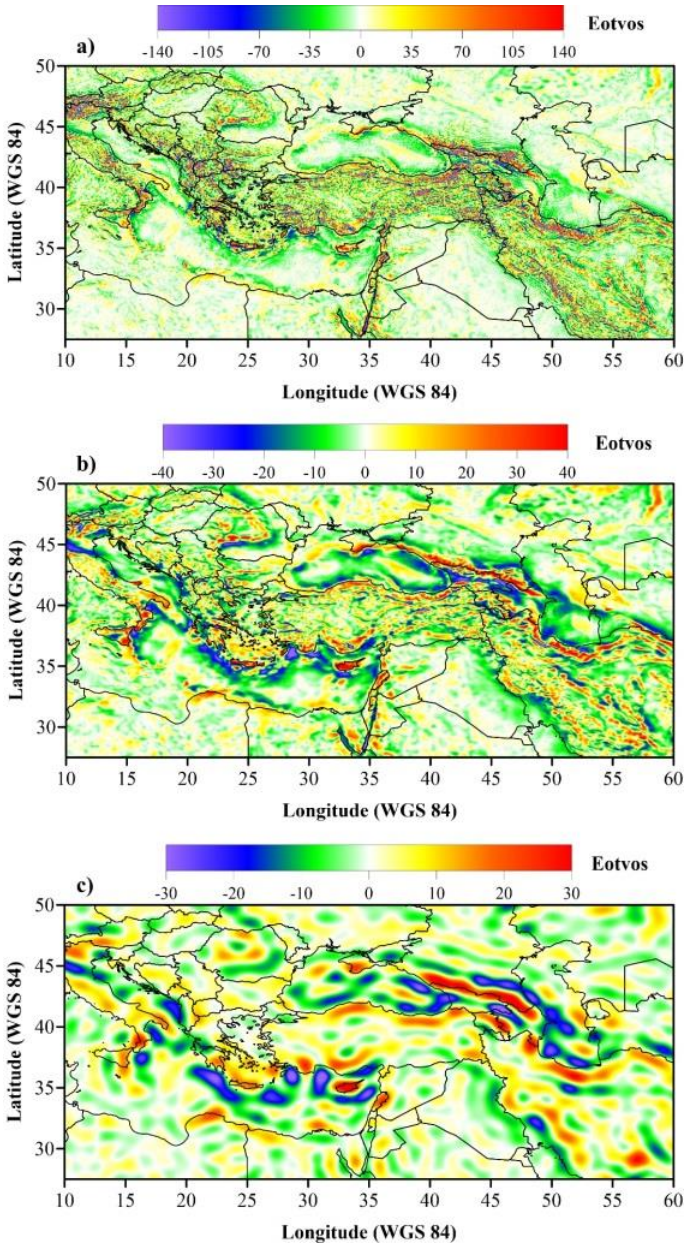

Figure 10. a) Tzz tensor of EGM2008 up to degree 2190, b) Upward continuation of Tzz tensor of EGM2008 and c) Tzz tensor of GOCE DIR R4 up to degree 240.

The initial mean depth value is needed for the inversion application of the Moho calculation. The radial averaged power spectrum method was applied in order to obtain the Moho anomaly to be used in the inversion. Critical wave numbers are important in determining bandpass limits and defined as points where the slope of the lines changes. This wave numbers are respectively, kr_1 = 0,025 km^{-1} ($\lambda_1 = 2\pi / kr_1$ = 251 km) and kr_2 = 0,106 km^{-1} ($\lambda_2 = 2\pi / kr_2$ = 59 km). From the slopes of these lines, the average depths of the interface boundaries were calculated as z_1=135 km (LAS), z_2=35 km, respectively (Figure 11).

After the power spectrum analysis of the spherical Bouguer gravity anomaly and decomposing the anomaly originating from Moho, then Moho depth map was obtained after inversion of this anomaly. The mean depth (z_0) approximately as 35 km obtained from the power spectrum analysis is used for the calculation of Moho depth in the 3DINVER program [22]. The program needs an initial knowledge of two parameters which are density contrast of the interface and the mean depth. Density contrast which is mantle density minus crust density was taken fixed as 0.4 g/cm^3. Earth's curvature was ignored as a parameter in the inversion formula for big area calculations but spherical approximation of gravity calculation could be an advantage because the spherical version uses a spherical shell of thickness equal to the orthometric height of the topography at the point of interest [23]. Moho depths were found at an average of 30 km in Western Anatolia, between 20-35 km in the Aegean Sea, between 35-45 km in Eastern Anatolia and between 10-20 km in Cyprus and its surroundings (Figure 12). The Moho variation between the depths of 40-50 km in the southeast of the study area and the Moho depth values of approximately 45 km in the Caucasus are quite compatible with the results of the studies of Lü et al., [24]. Lü et al., [24] obtained Moho depths with Pn seismic wave tomography method in their study. In

addition, the results of the continental crustal thickness in Turkey and its vicinity in the studies of Kayhan and Gülen [25] are in good agreement with the values obtained in this study.

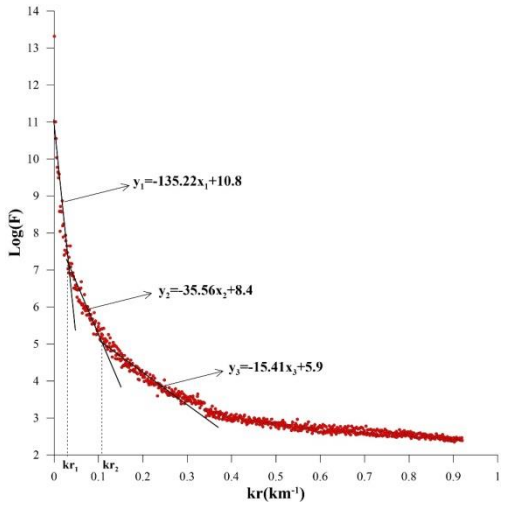

Figure 11. Radial power spectrum of Spherical Bouguer gravity anomaly.

The results are coherent with the Moho depth studies which was made in the eastern Anatolia by Pamukçu et al., [26]; in the western Anatolia by Pamukçu and Yurdakul [27] and in the eastern part of Mediterranean Sea by Doğru et al., [8]. In addition, Bilim et al., [28] obtained the crustal results for the Black Sea and the results of this study are compatible with their results. In addition, Moho depths from the GOCE Exploitation for Moho Modelling and Applications Project (GEMMA) [29] which has generated the first global high-resolution map of the boundary between Earth's crust and mantle based on data from the only GOCE satellite and An Updated Global Model of Earth's Crust (CRUST1.0) [30] model which has calculated from active source seismic studies on a 1-degree grid were shown in Figure 12. Although the data acquisitions are completely different, it is noticed that there is more coherence between the Moho depth of CRUST1.0 model and Moho depth obtained in this study especially in the marine areas. It can be said that the Moho depth result of GEMMA model presents best fit for marine areas but the results of Moho depth obtained in this study offers more relevant results especially eastern of Turkey with CRUST1.0 model.

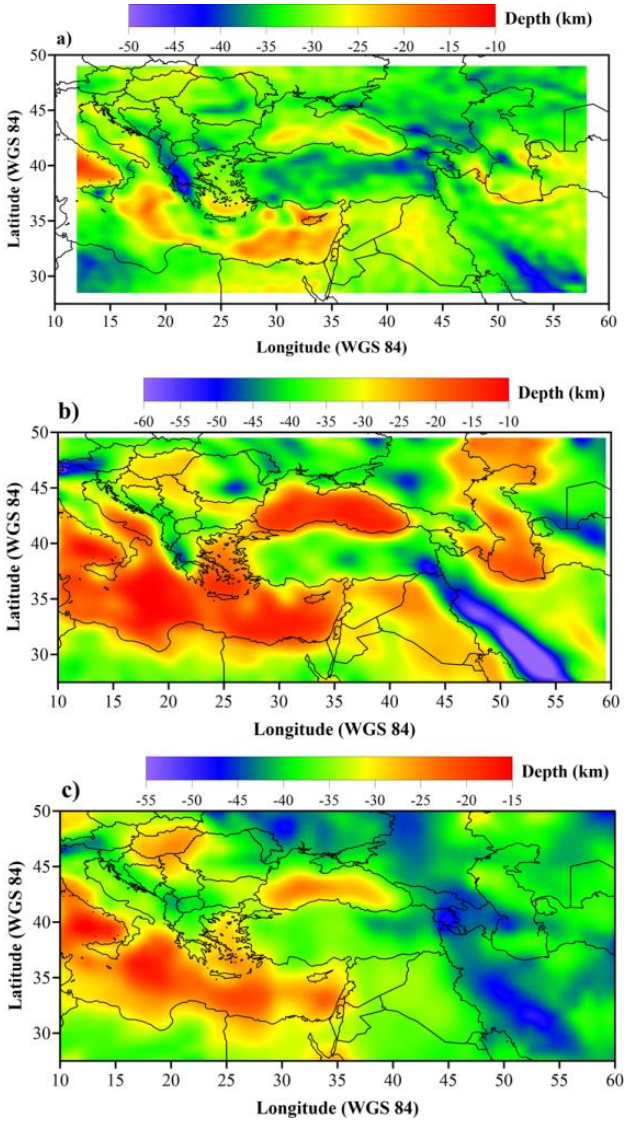

Figure 12. Moho depth variations of the study area from this study and other Moho models: a) Moho depth variation from this study, b) Moho depth from GEMMA model and c) Moho depth from CRUST1.0 model.

4. Conclusions

Within the scope of this study, the spherical free air gravity anomaly of the area was first calculated using satellite models. The combination of EGM2008 and GOCE DIR R4 models were used to calculate the spherical free air gravity anomaly. Afterwards, the spherical Bouguer gravity anomaly of the region was calculated with the help of the topography model. In addition, the gravity tensors of the region were calculated with only GOCE DIR R4 model (n: 240) and only EGM2008 (n: 2190) model. Thus, the effect of both deep structures and shallow structures could be observed. The Moho depth map of the study area from the west of Italy to the east of the Caspian Sea was obtained. Moho depth values of the region were obtained between 10 and 50 km. Moho depth values were observed to be compatible with the results of previous studies. Moho values were obtained in the range of 45 km in the Eastern Anatolia Region, around 30 km in the Western Anatolia, ~20 km around Cyprus, and 45-50 km in the south of the Caucasus and Iran (Figure 1).

A significant north-south anomaly variation was obtained especially along the Dead Sea fault, at upward continuation of Tyz and Tyy tensor of EGM2008 (Figures 8 and 9) and Tyz and Tyy tensor of GOCE DIR R4 up to degree 240 (Figures 8 and 9). Although this tectonic element has a predominantly lateral change, it is clear that there is a continuity of mass change in the vertical direction due to the change in the Tyz component.

An anomaly with a sharp positive-negative change in the direction of approximately northwest-southeast draws attention in the results of EGM2008 up to degree 2190, upward continuation of Txx, Txy, Txz, Tzz tensors of EGM2008 and Tzz tensor of GOCE DIR R4 up to degree 240 in Figures 5, 6, 7 and 10 between 35°-55° longitudes throughout the Caucasus (Figure 1). There is both a lateral and a vertical continuation of change along this one line in this area. The line of anomalies changing as smoothly as possible was observed throughout northernwest to southerneast trending and even to the Hellenic arc between 10°-25° longitudes in the results of EGM2008 up to degree 2190, upward continuation of Txy, Txz, Tzz tensors of EGM2008 and Tzz tensor of GOCE DIR R4 up to degree 240 in Figures 6, 7 and 10. This line also has the character of lateral and vertical change. However, the difference between this place and the Caucasus is that the positive-negative anomaly transition is not sharp.

In addition, negative amplitude changes in a wide area along the Hellenic arc in Figures 7 and 10 was observed in the results of EGM2008 up to degree 2190, upward continuation of Txz, Tzz tensors of EGM2008 and Txz, Tzz tensors of GOCE DIR R4 up to degree 240. The vertical continuity of the main character here reflects the subduction characteristics of the region very well. From this point of view, it is observed in Figures 7 and 10 that the line on which this tectonic element extending has continuity along the Mediterranean in the south of Anatolia. In fact, the anomaly amplitude value of this line increases in the positive direction and joins with the Bitlis Suture zone in the east in Figure 7.

Additionally, when Figure 5b is carefully examined the linear line with an average amplitude of 20 Eotvos coming from the 10° longitude west follows the Hellenic arc again merging with the Bitlis Thrust zone in the east and continues in the east. While Tzz and accordingly Txz variation in the vertical direction from the Hellenic arc is very dominant, the dominance of this line in Tzz in the vertical component cannot be observed when it approaches the Bitlis thrust in the east. Again, it is observed that there are parallel but same character changes towards Africa, especially around Cyprus in the south of this line (Figure 7).

Ethics Committee Approval and Declaration of Conflict of Interest

This article does not require ethics committee approval.

There is no conflict of interest with any person/institution in the prepared article.

Acknowledgment

The authors would like to thank the anonymous reviewers for his/her valuable comments.

References

[1] Dewey, J.F., Bird, J.M. 1970. Mountain belts and the new global tectonics. Journal of Geophysical Research, 75(14), 2625-2647. DOI:10.1029/JB075i014p02625.

[2] McKenzie, D. 1978. Active tectonics of the Alpine—Himalayan belt: the Aegean Sea and surrounding regions. Geophysical Journal International, 55(1), 217-254. DOI:10.1111/j.1365-246X.1978.tb04759.x.

[3] Jackson, J., McKenzie, D. 1984. Active tectonics of the Alpine—Himalayan Belt between western Turkey and Pakistan. Geophysical Journal International, 77(1), 185-264. DOI:10.1111/j.1365-246X.1984.tb01931.x.

[4] Angelier, J. 1978. Tectonic evolution of the Hellenic Arc since the late Miocene. Tectonophysics, 49(1-2), 23-36. DOI: 10.1016/0040-1951(78)90096-3.

[5] Angelier, J., Lyberis, N., Le Pichon, X., Barrier, E., Huchon, P. 1982. The tectonic development of the Hellenic arc and the Sea of Crete: a synthesis. Tectonophysics, 86(1-3), 159-196. DOI: 10.1016/0040-1951(82)90066-X.

[6] Anastasakis, G., Kelling, G. 1991. Tectonic connection of the Hellenic and Cyprus arcs and related geotectonic elements. Marine Geology, 97(3-4), 261-277. DOI: 10.1016/0025-3227(91)90120-S.

[7] Styron, R. 2019. GEMScienceTools/gem-global-active-faults: First release of 2019 (Version 2019.0). Zenodo. DOI:10.5281/zenodo.3376300.

[8] Dogru, F., Pamukcu, O., Gonenc, T., Yildiz, H. 2018. Lithospheric structure of western Anatolia and the Aegean Sea using GOCE-based gravity field models. Bollettino di Geofisica Teorica ed Applicata, 59(2), 135-160. DOI:10.4430/bgta0231.

[9] Bruinsma, S.L., Förste, C., Abrikosov, O., Marty, J.C., Rio, M.H., Mulet, S., Bonvalot, S. 2013. The new ESA satellite-only gravity field model via the direct approach. Geophysical Research Letters, 40(14), 3607-3612. DOI: 10.1002/grl.50716.

[10] Pavlis, N.K., Holmes, S.A., Kenyon, S.C., Factor, J.K. 2008. An earth gravitational model to degree 2160: EGM2008. EGU general assembly, 10, 13-18.

[11] Rexer, M., Hirt, C., Claessens, S., Tenzer, R. 2016. Layer-based modelling of the Earth's gravitational potential up to 10-km scale in spherical harmonics in spherical and ellipsoidal approximation. Surveys in Geophysics, 37(6), 1035-1074. DOI: 10.1007/s10712-016-9382-2.

[12] Bucha, B., Janák, J. 2013. A MATLAB-based graphical user interface program for computing functionals of the geopotential up to ultra-high degrees and orders. Computers and Geosciences, 56, 186–196. DOI: 10.1016/j.cageo.2013.03.012.

[13] Spector, A., Grant, F. 1970. Statistical models for interpreting aeromagnetic data, Geophysics, 35, 293–302. DOI: 10.1190/1.1440092.

[14] Pawlowski, R.S., Hansen, R.O. 1990. Gravity anomaly separation by Wiener filtering. Geophysics, 55(4), 539-548. DOI: 10.1190/1.1442865.

[15] Pawlowski, R.S. 1994. Green's equivalent-layer concept in gravity band-pass filter design. Geophysics, 59, 69–76. DOI: 10.1190/1.1443535.

[16] Sönmez, T. 2016. Doğu Marmara Bölgesinin litosfer dinamiklerinin EGM2008 gravite anomalileri, izostatik ve termomekanik analizlerle araştırılması. Yüksek Lisans Tezi, Kocaeli Üniversitesi Jeofizik Mühendisliği Bölümü, Kocaeli.

[17] Bhattacharyya, B. 1967. Some general properties of potential fi elds in space and frequency domain: a review. Geoexplor., 5, 127-143, DOI:10.1016/0016-7142(67)90021-X.

[18] Ruotoistenmäki, T. 1987. Estimation of depth to potential fi eld sources using the Fourier amplitude spectrum. Geol. Tutkimusk., 340, 84. DOI: 10.13140/RG.2.2.11841.61284.

[19] Parker, R.L. 1972. The rapid calculation of potential anomalies. Geophys. J. Int., 31, 447-455, DOI:10.1111/j.1365-246X.1973.tb06513.x.

[20] Oldenburg, D.W. 1974. The inversion and interpretation of gravity anomalies. Geophys., 39, 526-536, DOI:10.1190/1.1440444.
[21] Blakely, R.J. 1995. Potential theory in gravity and magnetic applications, Cambridge University Press. DOI: 10.1017/CBO9780511549816.
[22] Gómez-Ortiz, D, Agarwal, B.N. 2005. 3DINVER. M: a MATLAB program to invert the gravity anomaly over a 3D horizontal density interface by Parker–Oldenburg's algorithm. Computers & geosciences, 31(4), 513-520. DOI: 10.1016/j.cageo.2004.11.004.
[23] Vaníček, P., Tenzer, R., Sjöberg, L.E., Martinec, Z., Featherstone, W.E. 2004. New views of the spherical Bouguer gravity anomaly. Geophysical Journal International, 159(2), 460-472. DOI: 10.1111/j.1365-246X.2004.02435.x.
[24] Lü, Y., Ni, S., Chen, L., Chen, Q.F. 2017. Pn tomography with Moho depth correction from eastern Europe to western China. Journal of Geophysical Research: Solid Earth, 122(2), 1284-1301. DOI: 10.1002/2016JB013052.
[25] Kayhan, G., Gülen L. 2017. Türkiye ve civarında kıtasal kabuk kalınlığı araştırması.70th Geological Congress of Turkey, 26-27.
[26] Pamukçu, O.A., Akçığ, Z., Demirbaş, Ş., Zor, E. 2007. Investigation of crustal thickness in Eastern Anatolia using gravity, magnetic and topographic data. Pure and Applied Geophysics, 164(11), 2345-2358. DOI: 10.1007/s00024-007-0267-7.
[27] Pamukcu, O., Yurdakul, A. 2008. Isostatic compensation in western Anatolia with estimate of the effective elastic thickness. Turkish Journal of Earth Sciences, 17(3), 545-557.
[28] Bilim, F., Aydemir, A., Ateş, A., Dolmaz, M.N., Koşaroğlu, S., Erbek, E. 2021. Crustal thickness in the Black Sea and surrounding region, estimated from the gravity data. Marine and Petroleum Geology, 123, 104735. DOI: 10.1016/j.marpetgeo.2020.104735.
[29] Reguzzoni, M., Sampietro, D. 2015. GEMMA: An Earth crustal model based on GOCE satellite data. International Journal of Applied Earth Observation and Geoinformation, 35, 31-43. DOI: 10.1016/j.jag.2014.04.002.
[30] Laske, G., Masters, G., Ma, Z., Pasyanos, M.E. 2012. CRUST1. 0: An updated global model of Earth's crust. Geophys Res Abs, 14, 3743.